Journal of Materials Chemistry A

PAPER

View Article Online
View Journal | View Issue



Cite this: J. Mater. Chem. A, 2017, 5, 21435

# Compact high volumetric and areal capacity lithium sulfur batteries through rock salt induced nano-architectured sulfur hosts†

Matthew Li,‡[a] Yining Zhang,‡[a] Fathy Hassan,[a] Wook Ahn,[b] Xiaolei Wang,[a] Wen Wen Liu,[a] Gaopeng Jiang[a] and Zhongwei Chen *[a]

Tremendous efforts have been put into designing high gravimetric energy density lithium sulfur batteries (LIS) through increasing the areal sulfur loading in the cathode, however little to no attention has been paid to the volumetric energy density of LIS. Due to the low tap density of porous carbon as a common sulfur host, an excessively high electrode thickness per sulfur loading severely decreases the volumetric energy density to the point of little practical use. For the first time, a sulfur host with an engineered polymodal particle size distribution was utilized for compact high areal capacity sulfur electrodes. This material demonstrated the highest reported blade cast volumetric capacity of 495 mA h $cm^{-3}$ at 5.4 mA h $cm^{-2}$ while remaining true to traditional blade casting battery manufacturing processes. It demonstrated superior electrochemical activity at 0.1C by delivering capacities of 1010 mA h $g^{-1}$ at 10.2 mg $cm^{-2}$ and 1350 mA h $g^{-1}$ at 4 mg $cm^{-2}$ with good stability. Furthermore, even with its thin electrode profile of 86 μm at 4 mg $cm^{-2}$ capacities of 1103 mA h $g^{-1}$ and 972 mA h $g^{-1}$ at 0.2C and 0.5C were achieved, respectively.

Received 28th July 2017
Accepted 29th August 2017

DOI: 10.1039/c7ta06657k

rsc.li/materials-a



## Introduction

Lithium sulfur batteries (LIS) have become a popular area of research due to their high theoretical energy density of ~2600 W h $kg^{-1}$, which is about 5 times that of current lithium ion battery technologies.[1–4] However, the full potential of LIS is yet to be realized due to technical challenges such as the poor electrical conductivity of sulfur and the well-known polysulfide shuttle effect.[2] During discharge, PS dissolution from the cathode generates a concentration gradient, driving the diffusion of the PS from the cathode towards the lithium metal anode resulting in side reactions. Reported potential solutions comprise modification of electrolyte formulation,[5,6] addition of a PS impermeable layer onto the separator,[7,8] and engineering of new electrode materials,[3,9–11] with promising levels of success. Most publications in the LIS field, however successful, focus on electrodes with impractically low sulfur loadings of 1–2 mg $cm^{-2}$. Recent calculations by Peng *et al.* have provided some important insights into the relationship between areal sulfur loading and energy density of LIS, indicating a sulfur loading threshold of ~3.7 mg $cm^{-2}$ to compete with modern LIBs.[12] Although recent studies on high loading LIS have easily exceeded ~3.7 mg $cm^{-2}$, little attention has been paid to the constraints of potential end applications such as the battery volume in electric vehicles. Battery scientists must consider the volumetric energy density (VED) to ensure that the battery pack does not hinder or even compromise other aspects of the vehicle's system design.

The total number of publications that report on high loading blade cast LIS electrodes is surprisingly low, indicating that this electrode fabrication technology is slowly fading into obscurity.[10,13–18] Deviation from slurry blade casting techniques could require prohibitive reworking of traditional battery manufacturing processes and again brings back the problem of practicality. Although studying high loading LIS is crucial, it is equally important to be able to fabricate high loading electrodes while maintaining similar manufacturing processes to current LIB slurry blade casting techniques and acceptable volumetric energy densities. Solving the LIS system along with the consideration of these factors (areal capacity, volumetric energy density and manufacturability) enables LIS to be a "turn-key" battery solution that can be easily adopted and smoothly penetrate into the future electric vehicle battery market.

Keeping these design constraints in mind, we have synthesized a high tap density nitrogen doped porous carbon with a polymodal particle size distribution (poly-NPC), for high volumetric and areal capacity blade cast sulfur electrodes. With

[a]Department of Chemical Engineering, Waterloo Institute for Nanotechnology, 200 University Ave. W., Waterloo, Ontario N2L 3G1, Canada. E-mail: zhwchen@uwaterloo.ca

[b]Department of Energy Systems Engineering, Soonchunhyang University, 22 Soonchunhyang-ro, Shinchang-myeon, Asan-si, Chungcheongnam-do, 31538 Korea

† Electronic supplementary information (ESI) available. See DOI: 10.1039/c7ta06657k

‡ These authors contributed equally to this work.

particle sizes ranging from the nano to micron scale, the large particles allowed for the fabrication of robust electrodes at low binder contents while the inclusion of smaller diameter particles enables the fabrication of tightly packed electrodes. These particles possess macropores allowing lithium ions to be efficiently transferred within the large particle while PS can be trapped by nitrogen doping and the diffusion is limited by the space limitation effect of the small mesoporous structure. Through this design, we have successfully designed a promising blade cast electrode with high areal and volumetric capacities.

## Results and discussion

To engineer and achieve a robust high loading and blade cast sulfur electrode, the popular use of single nano-sized materials as sulfur hosts should be avoided. As such, much of recent work on blade cast electrodes has been based on micron sized materials.[19–21] However, work conducted on micron sized sulfur hosts for high loading LIS has produced electrode materials of limited tap density. Although micron sized particles have inherently higher tap density than the more popular nano sized sulfur hosts, there is still much room for improvement starting from the large volume of void space in between the micron sized particles. In this contribution, we have designed and synthesized poly-NPC which contains large micron sized particles while also incorporating smaller diameter particles to fill in the void gaps. This polymodal nature allows for a significantly more compact electrode when compared to other blade cast electrodes.

To synthesize such a material, one must understand the mechanism of polymerization of melamine and formaldehyde. Generally, polymerization reactions that produce insoluble particles are analogous to that of crystal growth.[22,23] There exists an initial seeding step where the solubility limit of the polymer is reached, inducing phase separation/precipitation (Fig. 1a). Depending on the surface chemistry of the seeds and the solvent, this is usually followed by a certain degree of aggregation to lower the surface energy and subsequent growth of aggregate particle size upon further polymerization. The seed in the case of this work is not pure MF but small nanocomposites of the silica template and MF resin or what we dubbed "seed composites". Without any modification of the surface charge, the hydroxyl group from the silica can offer a negative surface charge on the MF/silica composites, stabilizing the "seed composites". This is disadvantageous as it results in a narrower and smaller particle size distribution. To adjust the particle size distribution, we propose to control the surface charge of these "seed composites" through the addition of solid salt. The addition of solid NaCl introduces a high local concentration of $Na^+$ cations which can be adsorbed onto the surface of the exposed silica imbedded in these small composite particles (Fig. 1b) significantly destabilizing the system (Fig. 1c). To confirm this theory, zeta potential measurements are conducted. Samples with and without NaCl are synthesized and the zeta potential of the particle products is measured. The result indicates that the synthesized composite material without NaCl has a surface charge of around −9.95 mV (Fig. S1a†). The positive sodium ions added adsorb onto the surface of the negatively charged surface of seed particles (Fig. 1b) and lower the surface

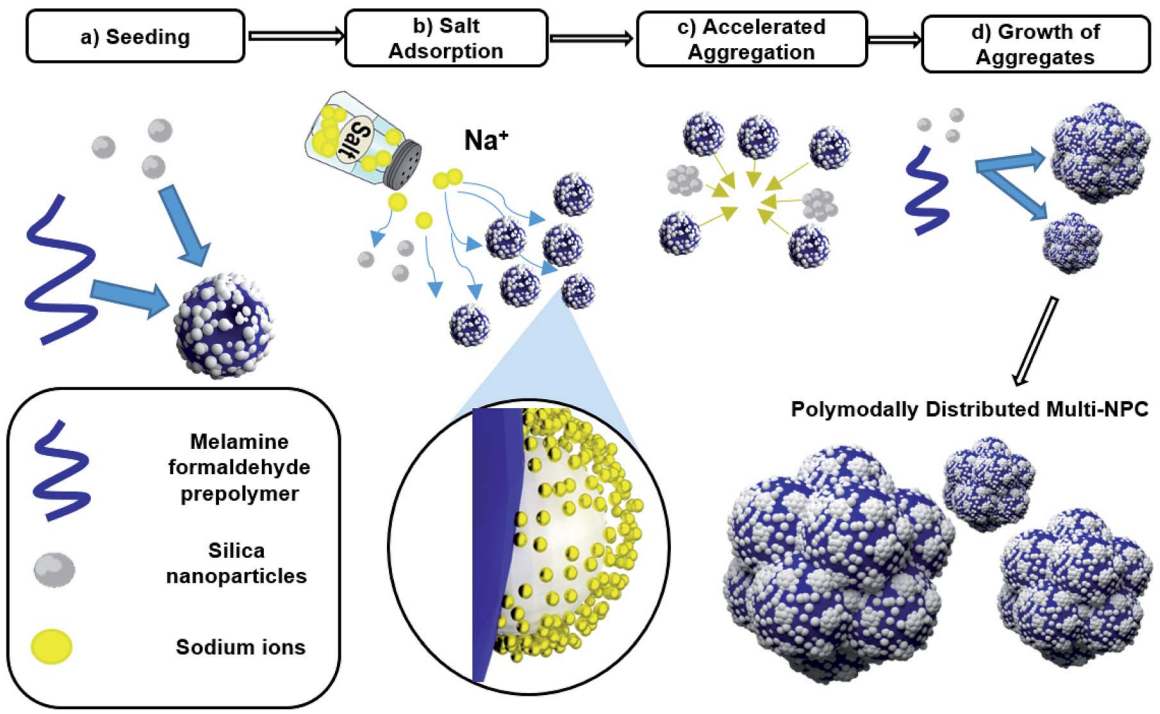


Fig. 1 Synthesis mechanism of poly-NPC: initial seeding of the polymer/silica composite (a), addition and adsorption of NaCl onto the surface of silica (b), aggregated particles of polymer/silica composite seeds (c) and growth of aggregates upon further polymerization (d).

 

charge to −1.67 mV (Fig. S1b†). Larger aggregates are produced early in the synthesis process; with an increased size of "seed composite" aggregates, an opportunity is created for the growth of much larger particles (Fig. 1d). It is noteworthy that from TEM imaging (Fig. S2†), these large particles do not appear to contain gaps in their structure, indicating that it is not the simple result of evaporation induced aggregation which would result in fragile particles. From SEM imaging (Fig. 2a), the particle size is on the order of microns with an apparent polymodal distribution. To investigate further, dynamic light scattering (DLS) is employed to provide a more reliable estimate, indicating that the particle size distribution is indeed in the micron range. More importantly, it appears that our speculation from SEM images was correct and the addition of NaCl did indeed produce a polymodal distribution. The smallest peak is at ~500 nm and the largest is at ~2 μm with signals up to 6 μm (Fig. 2b), whereas the sample without NaCl only resulted in a peak at 500 nm and a small peak at ~800 nm with absolutely no signal after ~1.2 μm (Fig. S3†). It should be noted that larger diameter particles could exist but were out of the detection range of our DLS. The solid NaCl added locally changed the ionic strength of the water and it was quickly adsorbed by the "seed composites". Due to the finite time of solvation, there is a delayed mixing of the solid NaCl in water which allows only a portion of the "seed composites" to experience the NaCl induced amplified aggregation. As the reaction proceeds, both the aggregated and non-aggregated particles will grow. Since the larger aggregates have a larger surface area per particle, they will grow at a rate that is faster than that of the smaller aggregates. This will cause divergences in the particle size distribution, which finally results in a polymodal particle size distribution in addition to an overall larger average final particle diameter.

After the removal of the silica template and the infiltration of 70% sulfur (confirmed by thermogravimetric analysis, Fig. S4†), the resulting material was fabricated into an electrode by blade casting. It was found that the poly-NPC/S composite was able to form a uniform and robust electrode up to 10.2 mg $cm^{-2}$ which was in alignment with previous use of micron sized hosts.[19] The most important and key benefit of poly-NPC was its packing density when fabricated into an electrode. If only one particle size was used for the electrode, then the amount of void space owing to the interparticle pores would be very large. This type of large spacing would require a large volume of electrolyte to fill during cell assembly and would not only lower the overall gravimetric energy density of the cell but also the volumetric energy density (VED). To ensure that sulfur electrodes were practically feasible for the system design of an electric vehicle and any other electrical system of interest, the VED must be increased. Since sulfur has a relatively low intrinsic mass density (2.01 g $cm^{-3}$) compared to commercial cathode materials, the VED is an especially crucial parameter in LIS and can be considered as the intrinsic Achilles heel of LIS technology. The VED in typical LIS work is often ignored and further decreased due to the use of low tap density porous materials. As per our design, to address the problem of a low VED, the cascading nature of the poly-NPC particle size distribution allows for a thinner more compact and electrochemically active electrode even at high sulfur areal loadings. Our work presents the first ever use of polymodally sized porous carbon in blade casting and achieved an exceptionally thin/compact high loading sulfur electrode. As shown in Fig. 2c, a cross-sectional SEM image of the electrode at ~8 mg $cm^{-2}$ areal sulfur loading exhibits an electrode thickness of ~200 μm (including a current collector of 23 μm). Our envisioned difference in the packing density between monomodally and poly-NPC's polymodally distributed particles can be found in Fig. 2d and e, respectively. The white spacing between the particles can be viewed as the void spaces that contribute to a lower electrode packing. From

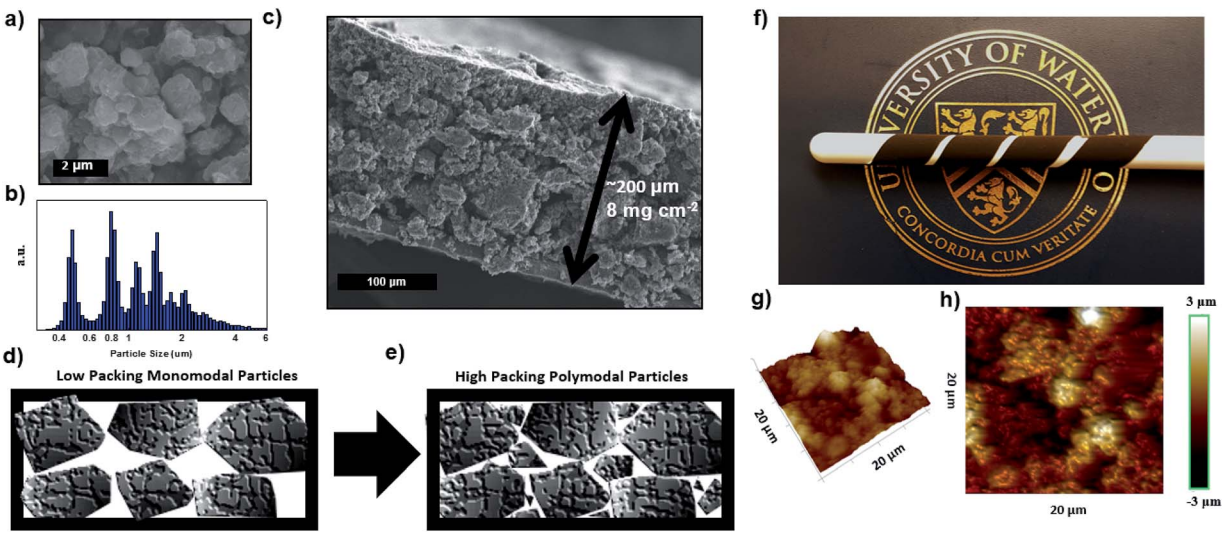


Fig. 2 SEM of poly-NPC prior to silica etching (a), poly-modal particle size distribution from DLS (b), the cross-sectional SEM image of an 8 mg $cm^{-2}$ sulfur loading electrode (c) envisioned difference in packing density between monomodal and polymodal particles (d and e). Photograph of the poly-NPC electrode demonstrating manufacturability (f), 3-dimensional atomic force microscopy surface plot of the poly-NPC electrode (g) and the corresponding 2D topographic plots (h).

Fig. 2d, the monomodal distribution of typical micron-particle based high loading sulfur electrodes exhibits a large interparticle void space (white spaces). Whereas when a polymodal particle size is used, the void space is drastically reduced, representing a highly packed electrode (Fig. 2e). Accordingly, in the cross-sectional SEM image of our electrode (Fig. 2c) smaller particles can be found in between the large particles, partially filling the voids. Fig. 2f illustrates the ability of an 8 mg $cm^{-2}$ electrode to keep its integrity even when wrapped around a high curvature (0.5 inch diameter) rod four times. This is a very important aspect of an electrode to be commercially adopted into roll-to-roll manufacturing methodologies of LIBs. Impressively, high loading poly-NPC electrodes as shown in Fig. 3a are achieved with only a mere 5 wt% binder, lower than those reported in most publications dealing with high loading sulfur electrodes.[15,24,25] To further characterize the poly-NPC electrode, atomic force microscopy (AFM) was employed. Fig. 2g displays a 20 μm by 20 μm three-dimensional plot of the topography of the poly-NPC elucidating the electrode surface features. From the topographic plot, it is apparent that poly-NPC possesses a relatively rough surface. Fig. 2h displays the corresponding 2D heat map topographic plots of poly-NPC. The rough surface allows for more surface area or more facets which the electrolyte can use to penetrate into the electrode. This is attributed to the intraparticle large pores throughout the poly-NPC structure. The presence of NaCl also agglomerates the 20 nm silica template, creating a large macroporous structure throughout poly-NPC.

Fig. 3a depicts the SEM image of a large-sized poly-NPC with intrinsic pores sizes of hundreds of nanometers in diameter. TEM imaging confirms that this large porous structure is throughout the whole particle (Fig. 3b). This observation introduces another critical role of surface charge modification with NaCl. In addition to agglomerating MF particles, the NaCl also agglomerates the 20 nm silica template, creating a large macroporous structure throughout poly-NPC. The micron-sized particles of poly-NPC are useful for providing ease of electrode fabrication in addition to a greater intraparticle diffusion resistance for PS. However, the intraparticle mass transfer dynamics of a typical micron sized particle can be sluggish for the lithium ions and is a disadvantage of using micron sized materials in any type of electrode. Mass transfer in and out of larger particles can increase the impedance in the cell, causing the cell to prematurely reach the cut-off. In addition to possessing the disadvantages of an average micron size, the polymodal nature of poly-NPC also creates a more compact electrode and should be even more tortuous for lithium ion mass transfer when compared to typical micron sized LIS electrodes. In contrast, this is circumvented by the macropores of poly-NPC. The macropores throughout the structure of poly-NPC ensure efficient mass transfer of Li-ions in and out of the micron sized particle which promotes high areal capacity discharge even with a more compact electrode profile.

Barrett–Joyner–Halenda (BJH) derived pore size distribution (PSD) is shown in Fig. 3c along with its $N_2$ adsorption/desorption isotherms (Fig. 3d), revealing a typical hierarchical porous pore size distribution with mesoporous peaks at ~20 nm and ~4 nm and is further corroborated by the Density Functional Theory (DFT) based pore size distribution shown in Fig. S5.† The peak in the BJH at ~20 nm pores corresponds well to the size of the silica template used. More importantly, the existence of ~20 nm implies that the creation of the macropores (formed by silica aggregation) only aggregated a portion of the silica population. The remaining crucial ~20 nm and ~4 nm pores allow poly-NPC to possess a high pore volume (2 $cm^3$ $g^{-1}$) with a sufficiently high surface area (926 $m^2$ $g^{-1}$) to accommodate sulfur into the poly-NPC structure as a thin layer. The exact mechanism of the formation of the ~4 nm pores is still unclear. We theorize that the salt-induced aggregation of the silica nanoparticles created interparticle voids between the silica particles, as shown in our geometric calculations in Fig. S6† and are preserved after template etching. The X-ray diffraction pattern (XRD) reveals that no sharp sulfur peaks are present indicating that sulfur was homogenously distributed (Fig. 3e).

To trap the PS within the particle and maintain enhanced cycle life, poly-NPC must possess additional properties such as nitrogen doping. Nitrogen doping has been previously shown to exhibit capabilities in adsorbing and retaining PS.[17,24,25] Since melamine is selected as the carbon precursor, the nitrogen content is found to be at a particularly high 15 at%, as shown in the XPS binding energy spectrum (Fig. S7†). Furthermore, electron energy-loss spectroscopy (Fig. 3f) reveals a homogenous distribution of nitrogen doping throughout poly-NPC. Although the mapped area is relatively small compared to the entire particle superstructure, it is worth noting that the loaded 70% sulfur appears to be distributed evenly throughout the poly-NPC porous network. In addition to trapping PS with nitrogen doping, the small mesopores (~4 nm) in the porous carbon can further enhance the ability of poly-NPC to limit PS diffusion out of the cathode.

To demonstrate the efficacy of our design, the electrochemical performance of the high areal loading poly-NPC electrodes from ~4–10 mg $cm^{-2}$ was studied. The given dry electrode thickness (including the current collector) at various sulfur loadings is presented in Fig. 4a, demonstrating the materials' exceptionally thin profiles. Electrodes at 6, 8 and 10 mg $cm^{-2}$ were discharged at 0.1C and delivered 1080, 1020 and 1010 mA h $g^{-1}$, respectively (Fig. 4b). Such a loading and

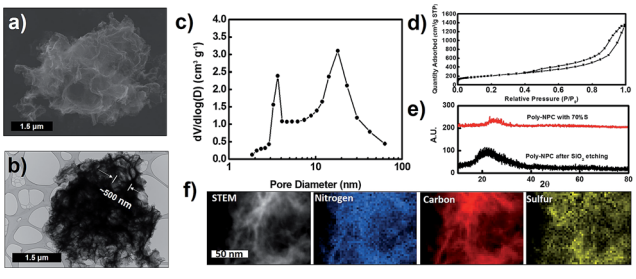


Fig. 3 SEM (a) and TEM (b) images of poly-NPC with 70% sulfur, pore size distribution of poly-NPC without sulfur (c), nitrogen adsorption and desorption isotherms (d), XRD pattern of poly-NPC with and without 70% sulfur (e) STEM and EELS mapping of nitrogen, carbon and sulfur ((f), left to right).

 

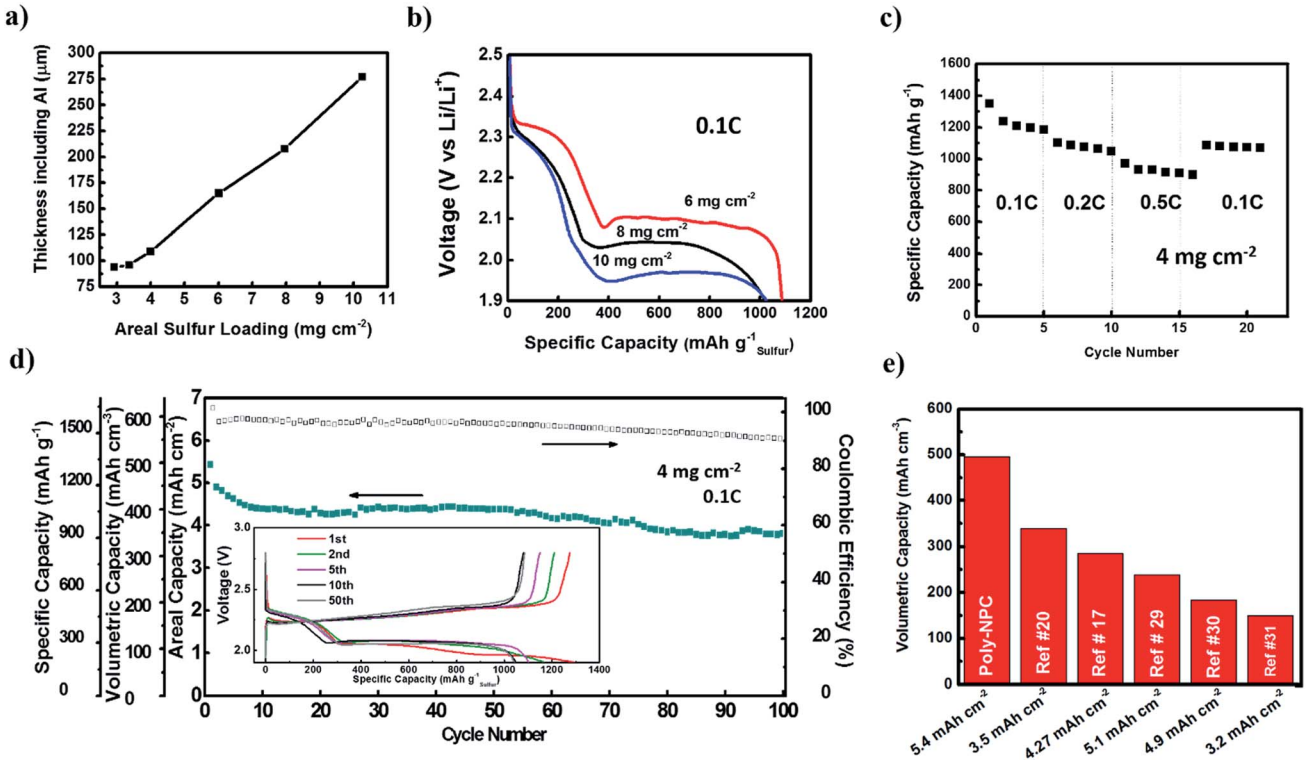


Fig. 4 Relationship between dried electrode thickness (including 23 μm thick carbon coated aluminum current collector) and areal sulfur loading (a) discharge capacity at 0.1C of poly-NPC at various loadings (b), rate performance of poly-NPC at various C-rates (c), cycle durability of poly-NPC at 4 mg cm$^{-2}$ (d), corresponding charge/discharge voltage profiles at the 1st, 2nd, 5th, 10th and 50th cycles (d inset) and comparison of the volumetric capacity of poly-NPC at 5.4 mA h cm$^{-2}$ to recently published blade cast high loading work[17,19,26–28] (e).

specific capacity are among the highest reported for blade cast sulfur electrodes to offer up to ~10.3 mA h cm$^{-2}$ at 0.1C with such a thin profile. To further emphasize the effect of the polymodally distributed electrode material on performance, electrodes of 4 mg cm$^{-2}$ are subjected to a rate performance test from 0.1 to 0.5C. These high loading electrodes can deliver 1103 mA h g$^{-1}$ and 972 mA h g$^{-1}$ at 0.2C and 0.5C, respectively (Fig. 4c). Stability is evaluated at 0.1C and 4 mg cm$^{-2}$ (Fig. 4d) with its corresponding charge/discharge voltage profile shown in the inset of Fig. 4d. It should be noted that the overpotential experienced by the 4 mg cm$^{-2}$ electrode appeared to be higher than that of the 6 mg cm$^{-2}$ electrode. This is most likely due to the higher 7.5 wt% binder content of the 4 mg cm$^{-2}$ electrode compared to the 5 wt% of the 6–10 mg cm$^{-2}$ electrodes. Similar to other work on high loading electrodes, to decrease the effect of a higher PS flux, a 0.1 mg cm$^{-2}$ poly-NPC coating (10 μm thick) was applied on the separator with the coated side facing the cathode.[14,24,29] In Fig. 4c the performance is normalized to the electrode area, electrode volume and S content. The 4 mg cm$^{-2}$ large particle electrode possesses a 1st discharge of more than 1350 mA h g$^{-1}$ (or 5.4 mA h cm$^{-2}$) stabilizing at around 950 mA h g$^{-1}$ in 100 cycles at 0.1C which is impressive given the thin profile of our electrode. The volumetric capacity (VC, in mA h cm$^{-3}$) can be used as an input to future battery volumetric density prediction models and allows us to compare volume based capacity. Taking into consideration the areal capacity of 5.4 mA h cm$^{-2}$ of the first discharge, this thickness corresponds to a VC of ~495 mA h cm$^{-3}$ (453 mA h cm$^{-3}$ if the interlayer coating is included). It is important to understand that a lower mass loading electrode typically yields a higher VC due to its typical higher sulfur utilization per unit volume. Therefore, the comparison of volumetric capacity is only meaningful if it is compared on a similar areal capacity basis. Fig. 4e compares the work done in this paper to other recently published studies (detailed cited data in Table S1†) which utilize blade cast LIS electrodes at similar areal capacities (5.4–3.5 mA h cm$^{-2}$). Owing to the polymodal particle size distribution, the volumetric capacity of poly-NPC is approximately 46% higher than the next leading work at 5.4–3.5 mA h cm$^{-2}$ areal capacity. Although this is still lower than the VC of the estimated commercial cathodes in the Panasonic NCR18650B LIBs cells (550 mA h cm$^{-3}$),[30] it is, to the best of our knowledge, the highest VC reported for LIS with an areal capacity that is comparable to those of commercial LIBs using traditional battery manufacturing methods.

## Conclusions

A polymodally distributed particle size porous carbon was synthesized through a silica templated melamine-formaldehyde resin solution. Sodium ions were used to control the surface of the seed polymer particles. The neutralized surface charge accelerated agglomeration during the polymerization process leading to a polymodal particle size distribution with a larger

average particle diameter. Taking advantage of this phenomenon, we fabricated a compact, high loading electrode of ~4–10.2 mg $cm^{-2}$. The 6, 8 and 10.2 mg $cm^{-2}$ electrodes delivered 1080, 1020 and 1010 mA h $g^{-1}$ at 0.1C, respectively. The 4 mg $cm^{-2}$ electrode fabricated from our polymodally distributed porous carbon material cycled at 0.1C achieved an impressive volumetric capacity of 495 mA h $cm^{-3}$ (5.2 mA h $cm^{-2}$ & 1350 mA h $g^{-1}$) which corresponds to at least a 46% improvement over previously published blade cast high loading sulfur electrodes. We hope this work can draw more focus on volumetric capacity from the LIS community.

# Methods

## Materials

Melamine, formalin solution, NaCl, HCl, $Na_2CO_3$, Ludox AS40, hydrofluoric acid (50%), and sulfur were purchased from Sigma Aldrich. The pre-blended electrolyte dimethoxyethane and 1,3-dioxolane at a 1 : 1 volume ratio with 1 M lithium bis(trifluoromethane)sulfonamide (LiTFSI) and 0.2 M lithium nitrate ($LiNO_3$) was purchased from Baden Aniline and Soda Factory (BASF). Carbon coated aluminum foil (current collector) was purchased from MTI corporation.

## Synthesis procedures

In a typical synthesis procedure of poly-NPC, 25 mL of distilled water was added to 6.3 g of melamine and 10 g of formalin solution, this was followed by the addition of 2 M sodium carbonate until a pH of 8.5 is reached. The obtained mixture was heated to 80 °C under stirring until the solution became clear. The solution was stirred for 15 minutes and allowed to naturally cool down to 40 °C. To follow, the template (silica) was added in the form of a 60 g solution of 5 wt% Ludox AS40, and was stirred at 40 °C for 20 minutes. 2 M HCl catalyst was added to the above mixture until the pH reached 4.5 and was stirred for an additional 10 minutes. During this time, 5 wt% (based on the weight of water) of solid NaCl was added into the reaction and stirred for an additional 5 minutes. Agitation was halted and the above solution was allowed to react for 4 hours under stagnant conditions. After 4 hours, there was a visible separation of precipitated polymerized melamine formaldehyde resin (MF) at the bottom while the bulk water phase remained in the top section. All mixing was done with a magnetic stir bar at 300 rpm. The top water phase was decanted and the remaining white slurry was dried in a 60 °C vacuum oven for 48 hours to remove remaining water. The obtained solid was then rinsed with distilled water to remove residual salt and filtered. After drying in a vacuum oven at 60 °C, the sample was heat treated at 180 °C for 12 hours to dry and obtain a near 100% conversion of the condensation polymerization reaction between melamine formaldehyde molecules. For carbonization, the sample was ramped from 30 °C to 900 °C at 5 °C $min^{-1}$ under an argon atmosphere. The silica template was subsequently removed by carefully stirring in 10% hydrofluoric acid solution for 48 hours. The remaining solid was carefully rinsed with water to remove the residual hydrofluoric acid.

Poly-NPC/sulfur composites were synthesized by the typical melt diffusion method, where the appropriate amounts of S and poly-NPC were mechanically mixed in a mortar. The mixture was then placed into a sealed argon filled Teflon lined autoclave and heated slowly to 155 °C and held isothermal for 12 hours.

As shown and implemented in many published studies on high loading LIS, a functional interlayer on the cathode surface could help suppress PS diffusion. Therefore, in this work a poly-NPC interlayer was also implemented by spraying a solution of 1 mg $mL^{-1}$ of poly-NPC (without sulfur) in ethanol. It is important to note that the loading of poly-NPC is only 0.1 mg $cm^{-2}$ and the thickness is only 10 μm.

## Physical characterization

Thermogravimetric analysis (TGA, TA instrument Q500) conducted under a nitrogen atmosphere was used to confirm the accurate percentage of S in the poly-NPC/S composite. The protocol entailed a heating rate of 5 °C $min^{-1}$ from 25 to 600 °C and maintenance at 600 °C for 2 hours. An Autosorb iQ-MP by Quantachrome was used to retrieve data which were analyzed using Brunauer–Emmett–Teller (BET) theory to calculate the surface area, and DFT theory to calculate the pore size distribution and pore volume of poly-NPC. A Zeiss Leo FESEM 1530 scanning electron microscope (SEM) was used to characterize the morphology of the material. Transmission electron microscopy (TEM) was conducted on a JEOL 2010F. X-ray photoelectron spectroscopy (XPS) was performed using a K-Alpha XPS spectrometer and dynamic light scattering (DLS) was performed on a DLS 135 Particle Size Analyzer with a 65 mW single mode red laser ($\lambda = 658$ nm) from Cordouan. Zeta potential measurements were done through electrophoresis with a WALLIS Zeta Potential from Cordouan. Atomic force microscopy (AFM) was performed on a Bruker Innova AFM. Thickness measurements were conducted using a 0–1 inch caliper from Mitutoyo.

## Electrochemical characterization

For electrochemical characterization, poly-NPC blade cast electrodes were fabricated with a water based slurry of 25% solid content. The mass ratio of each carbon/sulfur composite : carbon nanotube : LA 133 was 87 : 5.5 : 7.5 respectively for the 4 mg $cm^{-2}$ electrode and 89.35 : 5.65 : 5 for the electrodes from 6–10 mg $cm^{-2}$. The slurry was cast onto a carbon coated aluminum foil current collector with the desired mass loading. All electrodes were dried at 70 °C for 4 hours and cut into circular disk electrodes (diameter = 12 mm) before being transferred into an argon filled glovebox (Labstar MB10 compact, mBraun) with water and oxygen levels both under 0.5 ppm. The electrochemical performances were evaluated using a 2016 type coin cell. Electrochemical tests were performed with a Neware battery testing station. A lithium metal chip (Linyi Gelon LIB Co., Ltd) was used as the counter electrode and reference electrode for all tests. The separator used was Celgard 2500. For coin cell assembly, the electrolyte to sulfur ratio was maintained at 4 μL $mg_{sulfur}^{-1}$ for the cathode. The coin cells were cycled from 2.8 V to 1.5 V *vs.* $Li^+/Li$ for the rate performance tests and 2.8 V to 1.9 V *vs.* $Li^+/Li$ was used for cycle

 

life testing to avoid the irreversible decomposition of $LiNO_3$ on the cathode[31] at the cost of some capacity.

## Conflicts of interest

All authors declare no conflict of interest.

## Acknowledgements

This work was financially supported by the Natural Sciences and Engineering Research Council of Canada (NSERC), the University of Waterloo, and the Waterloo Institute for Nanotechnology. Special thanks to Dr Carmen Andrei and the Canadian Center for Electron Microscopy at McMaster University for the TEM images.

## References

1 W. Ahn, D. U. Lee, H. S. Song, S. H. Yeon, K. B. Kim and Z. Chen, *RSC Adv.*, 2015, **5**, 29370–29374.
2 X. Ji, K. T. Lee and L. F. Nazar, *Nat. Mater.*, 2009, **8**, 500–506.
3 W. Ahn, M. H. Seo, Y. S. Jun, D. U. Lee, F. M. Hassan, X. Wang, A. Yu and Z. Chen, *ACS Appl. Mater. Interfaces*, 2016, **8**, 1984–1991.
4 X. Wang, G. Li, J. Li, Y. Zhang, A. Wook, A. Yu and Z. Chen, *Energy Environ. Sci.*, 2016, **9**, 2533–2538.
5 M. Agostini, S. Xiong, A. Matic and J. Hassoun, *Chem. Mater.*, 2015, **27**, 4604–4611.
6 F. Wu, J. T. Lee, N. Nitta, H. Kim, O. Borodin and G. Yushin, *Adv. Mater.*, 2015, **27**, 101–108.
7 J. Balach, T. Jaumann, M. Klose, S. Oswald, J. Eckert and L. Giebeler, *Adv. Funct. Mater.*, 2015, **25**, 5285–5291.
8 W. Ahn, S. Lim, D. Lee, K. Kim, Z. Chen and S. Yeon, *J. Mater. Chem. A*, 2015, **3**, 9461–9467.
9 N. Jayaprakash, J. Shen, S. S. Moganty, A. Corona and L. A. Archer, *Angew. Chem., Int. Ed.*, 2011, **50**, 5904–5908.
10 G. Zhou, E. Paek, G. S. Hwang and A. Manthiram, *Nat. Commun.*, 2015, **6**, 7760.
11 M. Li, Y. Zhang, X. Wang, W. Ahn, G. Jiang, K. Feng, G. Lui and Z. Chen, *Adv. Funct. Mater.*, 2016, **26**, 8408–8417.
12 H.-J. Peng, W.-T. Xu, L. Zhu, D.-W. Wang, J.-Q. Huang, X.-B. Cheng, Z. Yuan, F. Wei and Q. Zhang, *Adv. Funct. Mater.*, 2016, **26**, 6351–6358.
13 M. A. Pope and I. A. Aksay, *Adv. Energy Mater.*, 2015, **5**, 1500124.
14 L. Qie, C. Zu and A. Manthiram, *Adv. Energy Mater.*, 2016, **6**, 1502459.
15 P. Bhattacharya, M. I. Nandasiri, D. Lv, A. M. Schwarz, J. T. Darsell, W. A. Henderson, D. A. Tomalia, J. Liu, J.-G. Zhang and J. Xiao, *Nano Energy*, 2016, **19**, 176–186.
16 H. Sohn, M. L. Gordin, M. Regula, D. H. Kim, Y. S. Jung, J. Song and D. Wang, *J. Power Sources*, 2016, **302**, 70–78.
17 Q. Pang and L. F. Nazar, *ACS Nano*, 2016, **10**, 4111–4118.
18 M. Yu, J. Ma, M. Xie, H. Song, F. Tian, S. Xu, Y. Zhou, B. Li, D. Wu, H. Qiu and R. Wang, *Adv. Energy Mater.*, 2017, 1602347.
19 D. Lv, J. Zheng, Q. Li, X. Xie, S. Ferrara, Z. Nie, L. B. Mehdi, N. D. Browning, J.-G. Zhang, G. L. Graff, J. Liu and J. Xiao, *Adv. Energy Mater.*, 2015, **5**, 1402290.
20 W. Li, Z. Liang, Z. Lu, H. Yao, Z. W. Seh, K. Yan, G. Zheng and Y. Cui, *Adv. Energy Mater.*, 2015, **5**, 1500211.
21 Y. Ma, H. Zhang, B. Wu, M. Wang and X. Li, *Sci. Rep.*, 2015, **5**, 14949.
22 Y. Wu, Y. Li, L. Qin, F. Yang and D. Wu, *J. Mater. Chem. B*, 2013, **1**, 204–212.
23 J. S. Downey, R. S. Frank, W. Li and H. D. H. Stover, *Macromolecules*, 1999, **32**, 2838–2844.
24 J. Song, M. L. Gordin, T. Xu, S. Chen, Z. Yu, H. Sohn, J. Lu, Y. Ren, Y. Duan and D. Wang, *Angew. Chem., Int. Ed.*, 2015, **54**, 4325–4329.
25 J. Song, T. Xu, M. L. Gordin, P. Zhu, D. Lv, Y.-B. Jiang, Y. Chen, Y. Duan and D. Wang, *Adv. Funct. Mater.*, 2014, **24**, 1243–1250.
26 Q. Pang, X. Liang, C. Y. Kwok, J. Kulisch and L. F. Nazar, *Adv. Energy Mater.*, 2016, **7**, 1601630.
27 S. Waluś, C. Barchasz, R. Bouchet, J. F. Martin, J. C. Leprêtre and F. Alloin, *Electrochim. Acta*, 2016, **211**, 697–703.
28 L. Zhu, W. Zhu, X.-B. Cheng, J.-Q. Huang, H.-J. Peng, S.-H. Yang and Q. Zhang, *Carbon*, 2014, **75**, 161–168.
29 J.-Y. Hwang, H. M. Kim, S.-K. Lee, J.-H. Lee, A. Abouimrane, M. A. Khaleel, I. Belharouak, A. Manthiram and Y.-K. Sun, *Adv. Energy Mater.*, 2016, **6**, 1501480.
30 M. Hagen, D. Hanselmann, K. Ahlbrecht, R. Maça, D. Gerber and J. Tübke, *Adv. Energy Mater.*, 2015, **5**, 1401986.
31 S. S. Zhang, *Electrochim. Acta*, 2012, **70**, 344–348.